Dissolution of SiO_2 in SiO_2-CaO-Al_2O_3 slags

by M. B. Folstad, M. Zhu, M. Tangstad

Affiliation:
Norwegian University of Science and Technology, Trondheim, Norway

Correspondence to:
M. B. Folstad

Email:
marit.b.folstad@ntnu.no

Dates:
Received: 19 May. 2026
Published: July. 2026

How to cite:
Folstad, M. B., Zhu, M., Tangstad, M. 2026. Dissolution of SiO_2 in SiO_2-CaO-Al_2O_3 slags. *Journal of the Southern African Institute of Mining and Metallurgy*, vol. 126, no. 7, pp. 395 – 404

DOI ID:
https://doi.org/10.17159/2411-9717/1021/2026

ORCiD:
M. B. Folstad
https://orcid.org/0000-0001-6862-8425
M. Zhu
https://orcid.org/0000-0002-5758-9747
M. Tangstad
https://orcid.org/0000-0001-9751-7716

This paper is based on a presentation given at the SAIMM Pyrometallurgy International Conference 2026, 26-28 May 2026, CSIR International Convention Centre, Pretoria, South Africa

Abstract

The dissolution rate of silica (SiO_2) into different compositions of SiO_2-CaO-Al_2O_3 slags was studied at 1500° C and 1550 °C under an inert atmosphere of argon. The results show that the dissolution process is controlled by mass transfer of SiO_2 in the slag. The experimental results were used to evaluate the dissolution rate, which was found to increase with increasing CaO/$Al2O_3$ ratios as well as with increasing temperature. Boltzmann–Matano analysis was applied to obtain a profile-based effective chemical inter-diffusivity. The extracted inter-diffusivity coefficients decrease systematically with increasing SiO2 content and fall in the range of ~10^{-12} – 10^{-13} m^2/s. These low values imply intrinsically slow diffusion-controlled SiO2 enrichment, so that approaching equilibrium is unlikely within the residence time of descending materials in industrial furnaces.

Keywords

Silica dissolution kinetics, SiO_2-CaO-Al_2O_3 slag, Silicon production, Boltzmann–Matano analysis, Slag viscosity

Introduction

Metallurgical silicon (Si) is industrially produced in submerged arc furnaces through carbothermic reduction of quartz (SiO_2). The overall mass balance is written as in Reaction 1, but the actual process is more complex and happens in several steps. In addition to the charge materials, oxide impurities are present in the furnace and will react and interact with the charge.

$$SiO_{2\,(s)} + 2C_s = Si_l + 2CO_g \quad [1]$$

The amount of accumulated slag in the furnace is an important factor in deciding the productivity of the furnace, and significant variations have been observed between different furnaces during furnace excavations over the last 15 years (Jusnes, 2020; Ksiazek, 2018; Ksiazek et al., 2013; 2018; Tangstad et al., 2014; Tranell et al., 2010). Accumulated slag is typically found along the furnace walls, sometimes extending all the way up to the charge top, and at the furnace bottom. The slag is more viscous than the Si metal and more slag accumulated will therefore affect the fluid flow in the furnace. A too thick layer of accumulated slag along the furnace walls hinders the raw materials from descending and, hence, narrows the reaction route. Accumulated slag at the bottom of the furnace affects the tapping process, as it may hinder the metal flow towards the tap-hole and it can also clog to the tap-hole.

The slag in the Si furnace mainly contains SiO_2, CaO, and Al_2O_3. Figure 1 shows the phase diagram of this system. It is found that the accumulated slag in the upper parts of the furnace generally has a higher SiO_2 content compared to the slag accumulated further down in the furnace (Folstad, 2023). The viscosity of the slag has a great impact on how the materials move through the furnace. It is preferable to have a lower viscosity to ensure a good mass flow and let the raw materials react as they descend. An increasing amount of SiO_2 in the slag will increase the viscosity. The amount of SiO_2 in the slag will also affect the liquidus temperature. For slags with a high amount of CaO or $Al2O_3$, the addition of SiO_2 lowers the liquidus temperature. However, for slags with SiO_2 > 60 wt%, more SiO_2 to the system will decrease the liquidus temperature. The Si furnace is normally divided into a low temperature zone that includes the higher parts of the furnace and along the furnace walls, and a high temperature zone

in the lower parts of the furnace around the electrode tip (Schei et al., 1998). This means that the slag inside the Si furnace experiences different temperatures, depending on where it is in the furnace. Figure 2 shows an illustration of the Si furnace, including the main zones and approximate temperatures at the different positions. The temperatures are based on COMSOL simulations from Myrhaug (2020) and temperature measurements from Johansen et al. (1998), and Ksiazek et al. (2021). The highest temperatures can be found right below the electrodes around the arc. Below the cavities is the metal bath, which holds a temperature around 2000 °C. With increasing distance from the arc, towards the furnace lining and upwards, the temperature decreases. The temperature in the charge area is normally around 900 °C – 1200 °C, but during challenging conditions the temperature has been measured up to 1700 °C.

Based on these temperatures, slag is not expected to be found in the upper parts of the furnace during normal operation. However, the existence of slag higher up in the inactive zone could be explained by a high crater pressure pushing the slag from the bottom to the lining, and up towards the charge top. Kadkhodabeigi (2011) modelled the effect of the crater pressure on the melt flow pattern in the furnace bottom and found that a high crater pressure pushes the melt towards the furnace walls. This model does not include slag in the melt, which has a higher viscosity than the metal. However, the findings of slag higher up in the furnace in the inactive zone indicate a sufficient high crater pressure to move the slag in the same way as the metal to the furnace wall and upwards. The objective of this paper is to investigate the dissolution of descending quartz into accumulated SiO_2-CaO-Al2O_3 slag as a potential cause for the increased SiO_2 levels observed in the upper parts of the furnace. To evaluate this, we have investigated the dissolution rate at 1500 °C and 1550 °C for three different slag compositions relevant to silicon production.

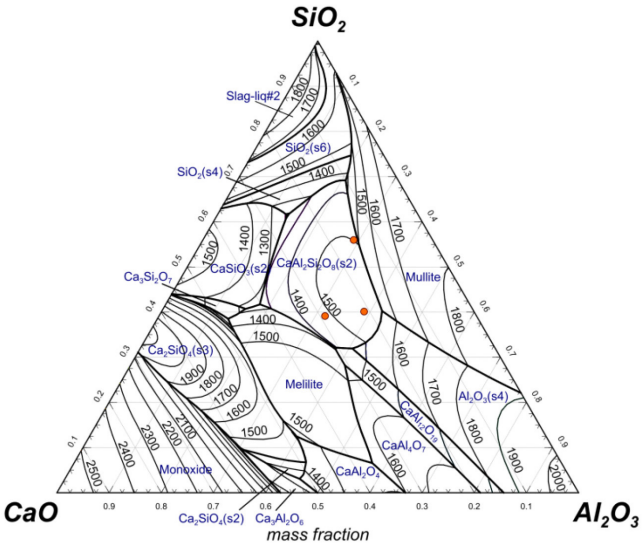

Figure 1—The SiO_2-CaO-Al_2O_3 ternary phase diagram, generated using FactSage 8.4

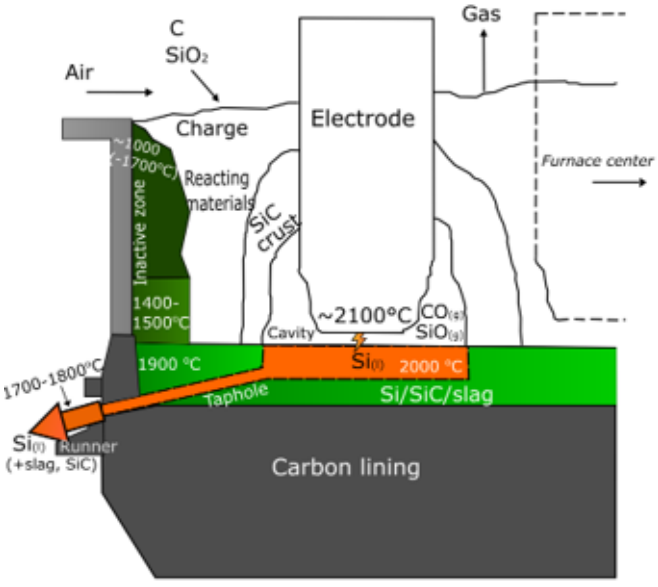

Figure 2—Illustration of a Si furnace including the main zones and approximate temperatures at different positions. The temperatures are based on modelled temperatures from Myrhaug (2020), and temperature measurements from Johansen et al. (1998) and Ksiazek et al. (2021)

Previous studies on SiO2 dissolution kinetics

The literature available on SiO_2 dissolution in SiO_2-CaO-Al_2O_3 slag relevant to Si production is limited. Most research has been carried out on the reaction related to the steel industry. Experimental studies have found that the dissolution process is controlled by diffusion in the liquid slag. Several researchers have also deduced the diffusivity from dissolution rate data (Feichtinger et al., 2014; Gou et al., 2023; Majdič, Wagner, 1965; Ren et al., 2022; Samaddar et al., 1964). A short summary of these diffusion coefficients, together with the respective slag compositions, temperatures, and viscosities, is presented in Table 1.

The first studies on the dissolution behaviour were done by dipping solid SiO_2 in slags for a fixed time. Samaddar et al. (1964) and Oishi (1965) studied the dissolution of fused silica at temperatures between 1350 °C and 1500 °C. They found that the dissolution of vitreous SiO_2 was controlled by transport within the liquid boundary layer, and that the CaO/Al_2O_3 ratio increased at the interface. The diffusion coefficients were calculated based on slag characteristics for the slag composition of 40% SiO_2 – 40% CaO – 20% Al_2O_3 and were found to be in the range of 10^{-12} m2/s.

Later studies were conducted in high-temperature confocal scanning laser microscopy (HT-CSLM). Feichtinger et al. (2014) studied the dissolution of amorphous SiO2 particles in six different compositions of SiO_2-CaO-Al_2O_3 slag with SiO_2 concentrations between 37.1% and 50.5% at 1450 °C. They found that the shape of the dissolution curves varied as a function of the slag composition. The dissolution pattern was strongly affected by slag viscosity, not by the concentration or the activity of SiO_2. Slags with higher viscosities resulted in longer dissolution times. The patterns were compared with the shrinking core model, and they showed that this model could not represent the dissolution behaviour observed in their study. The effective binary diffusion coefficient was calculated from Fick's second law of diffusion.

Ren et al., (2022) also studied the dissolution mechanism of SiO_2 in the HT-CSLM for three different slag compositions at temperatures from 1520 °C to 1580 °C. Their study confirms that the dissolution of SiO_2 inclusions is primarily controlled by mass transfer in the slag phase rather than the chemical reaction at the interface. They also found that decreasing the CaO/Al_2O_3 ratio also decreases the diffusion coefficient, and that increasing temperature increases the diffusion coefficient. From their results, the dissolution rate is affected by both the concentration gradient and the interface area. Gou et al., (2023) studied the dissolution of SiO_2 inclusions

with varied size using the CSLM and found that with increasing initial size of SiO_2 inclusions increased the dissolution time in a low silica slag with composition 8.3% SiO_2 – 50% CaO – 41.7% Al_2O_3 at 1500 °C. Both Ren et al., and Gou et al., found a linear relationship between the dissolution rate and a ratio of concentration difference and slag viscosity ($\Delta C/\eta$). This linear correlation suggests that viscosity is the dominant factor in the dissolution kinetics.

Kristiansen (2022; 2023) studied the dissolution rate of industrial quartz into three compositions of SiO_2-CaO-Al_2O_3 slags relevant for the Si production. His research indicated that the dissolution was controlled by the chemical reaction and that the dissolution was driven by the basicity of the slag, isothermal holding time, and the interface area of the liquid slag. He found the activation energy for two slags of 50% SiO_2 - 21% CaO – 29% Al_2O_3, and 62% SiO_2 - 20% CaO – 18% Al_2O_3 to be 119.9 kJ/mol and 83.7 kJ/mol, respectively.

Materials, equipment and methods

Based on slag compositions found in accumulated slag samples in industrial Si furnaces (Folstad, Tangstad, 2021; Jusnes et al., 2021), we utilised three different SiO_2-CaO-Al_2O_3 slag compositions with two different CaO/Al_2O_3 ratios. We melted mixtures of SiO_2, limestone ($CaCO_3$) and Al_2O_3 powder in an induction furnace. Table 2 presents the purity of the powders and the suppliers. To ensure a homogenous slag phase, we remelted the mixtures three times at temperatures up to 1800 °C, which is significantly above the expected liquidus temperatures for the different slag compositions. Table 3 lists the compositions of all three slags, their respective liquidus temperatures T_{liq}, and their viscosities η at 1500 °C and 155 °C. The compositions are plotted in the ternary phase diagram in Figure 1.

For the dissolution experiments, we used SiO_2 substrates with a 10 mm diameter and 3 mm height. To prevent the slag from spreading during the heating experiments, we coated the edges of the substrates with a thin layer of boron nitrate. The preparation involved pressing 0.6 g of slag powder into pellets, which were then placed on top of the SiO_2 substrates. We conducted the dissolution experiments in a sessile drop furnace, heating the samples up to 1500 °C or 1550 °C at a rate of 50 °C/min. This temperature exceeds the liquidus temperature for Slag 1 and 3. Isothermal holding times varied from 0 to 60 minutes, where 0 minutes indicate no isothermal holding time. The sessile drop furnace utilises graphite heating elements, and a B-type thermocouple measures the temperature. Figure 3 shows the SiO_2 and slag before the experiment, and the slag after experiment.

We used an EPMA, JEOL JXA 8500 to investigate the SiO_2 and slag after the sessile drop furnace experiments. After the furnace runs, we mounted the samples in epoxy and then prepared a vertical cross section in the centre of each sample. We imaged the cross sections with EPMA and determined the oxide compositions via a wavelength-dispersive X-ray spectrometer (WDS) to quantify the different elements in the samples.

Table 1
Summary of earlier research on the dissolution of SiO_2 in SiO2-CaO-Al2O3 slag. D is the diffusion coefficient and η is the viscosity.

Author	Slag composition			T [°C]	D [m^2/s]	Viscosi-ty [cP]	Comment
	SiO_2	CaO	Al_2O_3				
Samaddar et *al.*, (1964).	40	40	20	1350	$1.8\cdot10^{-12}$	2311	Forced convection.
				1390	$3.2\cdot10^{-12}$	1652	
				1425	$4.5\cdot10^{-12}$	1251	
				1500	$6.5\cdot10^{-12}$	720	
Majdič and Wagner (1970),	45	38.5	16.5	1500	$2.8\cdot10^{-10}$	896	D calculated with Fick's second law of diffusion.
Feichtinger et al., (2014).	54.6	34.1	10.6	1450	$4.4\cdot10^{-11}$	2410	
	50.5	38.3	10.6		$8.5\cdot10^{-11}$	1250	
	45.3	43.7	10.4		$1.8\cdot10^{-10}$	1080	
	42.8	46.6	10.8		$2.4\cdot10^{-10}$	1020	
	37.1	36.4	26.5		$3.8\cdot10^{-11}$	600	
	42.3	38.8	18.9		$6.0\cdot10^{-11}$	470	
Ren et al., (2023).	48.4	43.6	5.0*	1520	$3.3\cdot10^{-10}$	305	* +3.0% MgO.
				1550	$3.9\cdot10^{-10}$	258	
				1580	$4.0\cdot10^{-10}$	219	D calculated from modified version of the rate equation for mass-transport-controlled dissolution.
	45.8	41.2	10.0*	1520	$2.0\cdot10^{-10}$	356	
				1550	$2.3\cdot10^{-10}$	299	
				1580	$2.1\cdot10^{-10}$	252	
		38.8	15.0*	1520	$1.4\cdot10^{-10}$	428	
	43.2			1550	$1.5\cdot10^{-10}$	356	
				1580	$1.3\cdot10^{-10}$	298	

Table 2

The raw materials used in Slag 1-3 for the dissolution experiment

Product	Supplier	Purity
SiO_2	ThermoFisher Scientific (2024)	>99.9%
Limestone ($CaCO_3$)	FranzeFoss Minerals AS (2024)	>99.7%
Al_2O_3	ThermoFisher Scientific (2024)	>99.9%

Table 3

SiO_2- CaO-Al_2O_3 slags used in the dissolution experiments. Compositions are given in wt%; liquidus temperatures (Tliq) and viscosities for the slags are calculated using FactSage 8.4

	SiO_2	CaO	Al_2O_3	C/A	Tliq	Viscosities [cP]	
					[°C]	1500 °C	1550 °C
Slag 1	56	15	29	½	1497	45 636	25 012
Slag 2	40	21	39	½	1552	8753	5118
Slag 3	39	29	32	1	1467	3083	2975

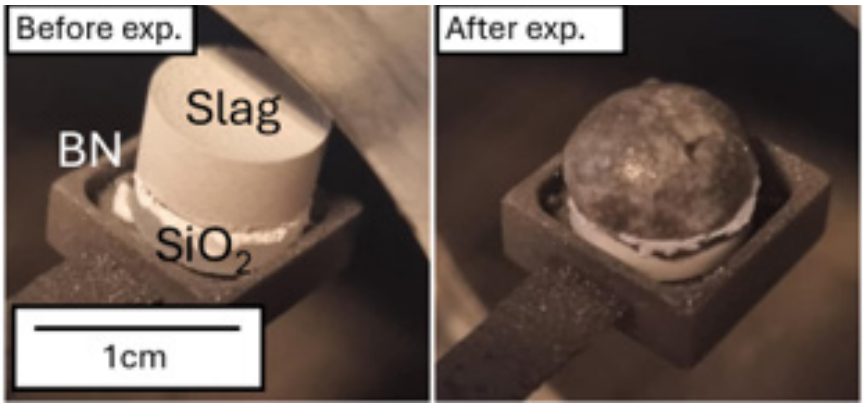

Figure 3—Slag and SiO2 before sessile drop experiment and slag after dissolution experiment

Results and discussion

This chapter presents the experimental findings on the dissolution of SiO_2 in SiO_2-CaO-Al_2O_3 slags and discusses their implications for industrial furnace operations. The first section evaluates the concentration profiles obtained via EPMA-WDS to verify if the transport is diffusion-controlled. Subsequently, Boltzmann-Matano analysis is used to quantify the concentration-dependent diffusivity and the activation energy of the process. Finally, these kinetic data are linked to slag viscosity and residence time to explain the accumulation of SiO_2-rich slag in the inactive zones of the furnace.

Figure 4 presents cross-sectional images of four dissolution experiments with the SiO_2 and Slag 1 after isothermal holding times ranging from 0 to 60 minutes at 1500 °C. The SiO_2 concentration in the slag was measured in the slag phase using EPMA-WDS analysis, starting from the SiO_2 interface and extending 140 µm into the bulk slag. The resulting concentration profiles are shown in Figure 5 as a function of distance from the interface. Beyond this distance, the slag composition remained equal to the initial concentration. One curve is shown in light grey. This represents Slag 1 with a 30-minute isothermal holding time and is considered an outlier. These graphs show a distinct concentration gradient near the interface, and the SiO_2-rich zone extends progressively further into the slag with time while approaching a far-field plateau. This behaviour is consistent with the growth of a transport boundary layer and suggests diffusion-dominated dissolution in the early stages. This is consistent with earlier research (Feichtinger et al., 2014; Gou et al., (2023); Majdič, Wagner, 1970; Oishi et al., 1965; Ren et al., 2022; Samaddar et al., 1964). Several of the concentration profiles in Figure 4 do not converge towards the initial bulk concentration of the slag. This is because the slag solidified into two distinct phases during cooling, as can be observed in the cross-sectional images. To account for this phase separation in the calculations, an average concentration was utilised. By applying this average concentration, the measured values converge towards the initial bulk concentration of the slag.

By fitting the dissolution profile, it was found that a constant-diffusivity assumption can only reproduce the near-interface region within the first 20 µm, but it systematically underestimates the concentration penetration at larger distances. This indicates that the mass transfer varies strongly with local SiO_2 content, implying a strongly composition-dependent effective diffusivity that is

Dissolution of SiO_2 in SiO_2-CaO-Al_2O_3 slags

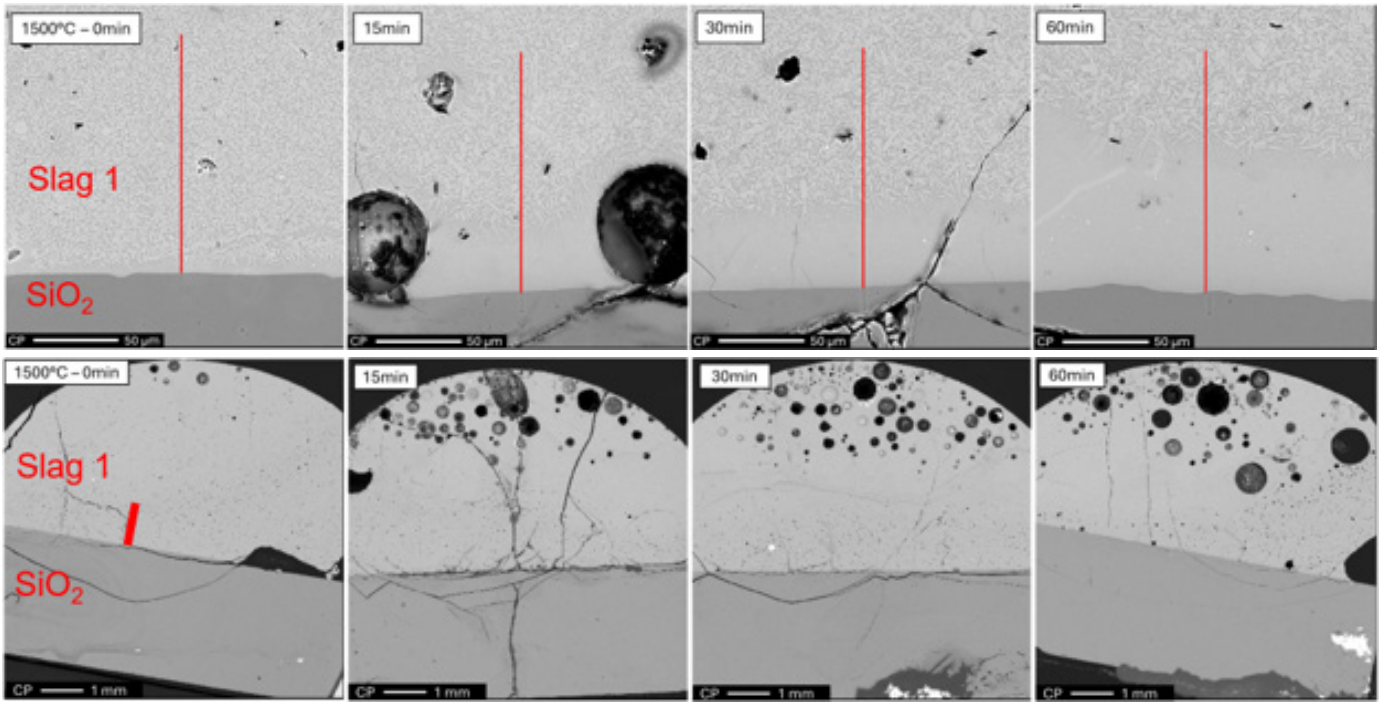

Figure 4—Cross-section images of SiO2 and Slag 1 captured with EPMA after different holding times from 0-60 minutes at 1500 °C

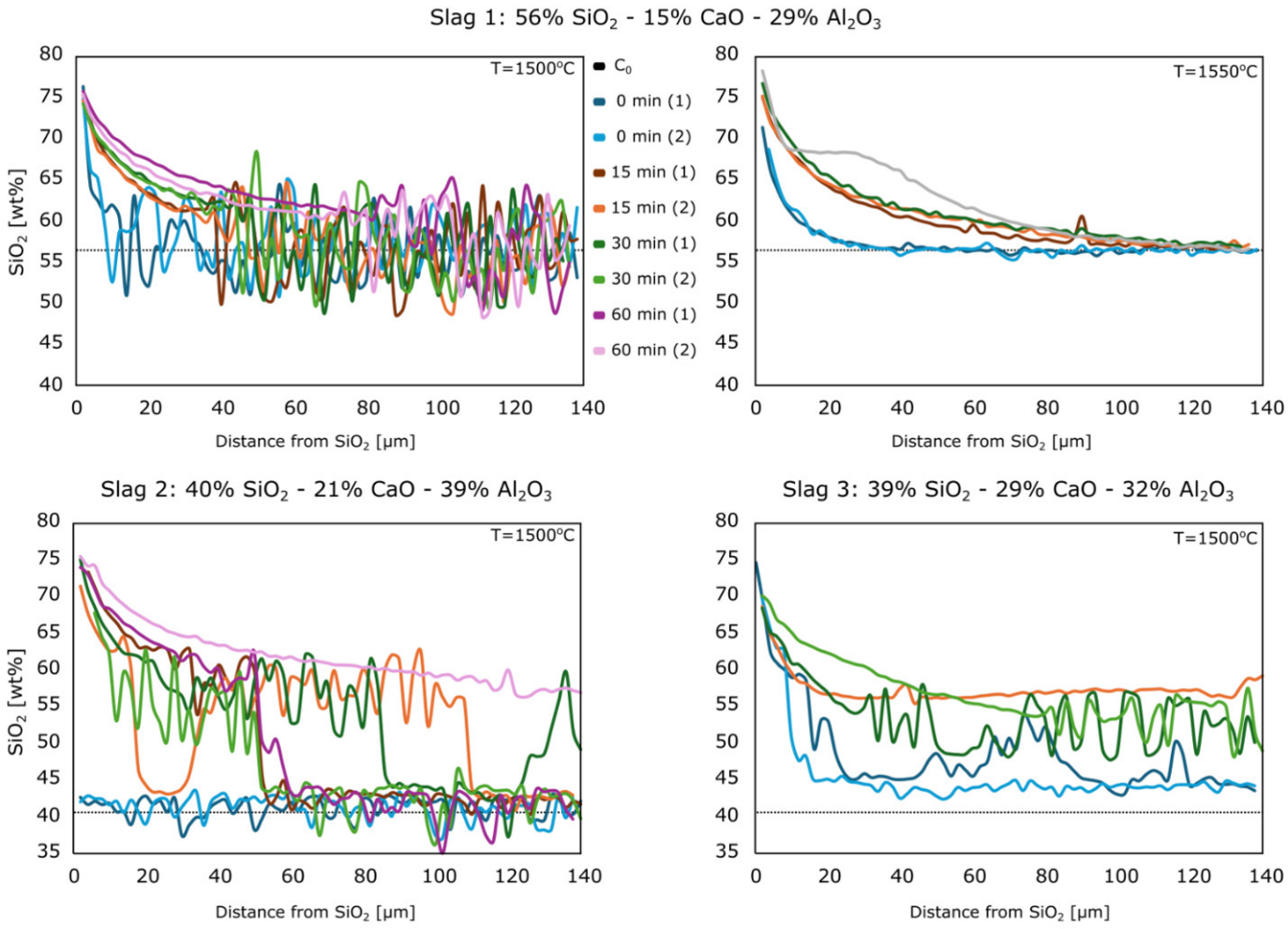

Figure 5— The experimental results given as SiO_2 concentration as a function of the distance from the SiO_2 interphase of the vertical cross sections. The SiO_2 concentration was measured in the slag phase using EPMA-WDS analysis. One curve is shown in light grey. This represents Slag 1 with a 30-minute isothermal holding time and is considered an outlier

consistent with higher values at lower SiO_2 contents. To quantify this composition dependence from the measured concentration profiles, Boltzmann–Matano (B–M) analysis was employed to invert the experimental C(x,t)-data and extract an effective concentration-dependent diffusivity $\tilde{D}(C)$ (Heo, Park, 2022).

The B–M approach assumes a diffusion-dominated, self-similar concentration field, such that the concentration profiles measured at different times should have the same shape when plotted against the scaled coordinate η, from Equation 2 (Crank, 1979). If diffusion is the dominant transport mechanism, the data curves from different time intervals should collapse onto a single 'master curve' in η-space; therefore we first perform a Boltzmann collapse test to verify this self-similarity assumption and to identify the time and composition ranges over which B–M inversion is applicable.

$$\eta_{BM} = \frac{x}{\sqrt{t}} \quad [2]$$

Where η is a time-independent position variable, x is the distance from the interface and t is the time.

Figure 6 shows the B-M screening results for the SiO_2 dissolution profiles, including the raw concentration profiles and the corresponding Boltzmann-scaled plots (C vs. $\eta_{BM}=x/\sqrt{t}$) used to assess self-similarity.

The analysis shows that the curves from Slag 1 at both 1500 °C and 1550 °C exhibit a strong collapse. This behaviour is consistent with diffusion being the main driver near the interface and supports the applicability of B-M analysis for determining the concentration-dependent diffusivity $\tilde{D}(C)$ for this composition. Similarly, the curves for Slag 3 collapse reasonably well near the interface for two profiles, making a diffusion-controlled mechanism plausible, albeit with caution. Slag 2 collapses poorly. This poor fit suggests that Slag 2 is unique and that additional process, such as convection or phase-related effects, may contribute. This slag has a higher liquidus temperature compared to Slag 1 and 3, and is most likely only partly melted at the experimental temperature of 1500 °C. Because B-M analysis assumes a homogeneous slag phase, it cannot accurately be applied to Slag 2, indicating that the dissolution mechanism for this composition is different.

Figure 7 shows the concentration-dependent effective diffusivity extracted from the SiO_2 dissolution profiles of Slag 1 and Slag 3 using B–M inversion, reported as the median with an interquartile range band across the available profiles. For all conditions, $\tilde{D}(C)$ decreases systematically with increasing SiO_2 content, with values spanning roughly from 10–12 to 10^{-13} m^2/s over the composition intervals around 65 wt% SiO_2. This strong composition dependence is consistent with the expectation that SiO_2-enrichment increases melt polymerisation and viscosity, thereby reducing species mobility. Furthermore, the diffusivity of Slag 1 increases as the temperature increases from 1500 °C to 1550 °C.

Compared with literature values reported for lower-viscosity slags from Feichtinger et al. (2014) and Ren et al. (2022), who reported values in the range of 10^{-10} - 10^{-11} m^2/s for temperatures between 1450 °C and 1580 °C, the diffusivities obtained here are lower. However, it is worth noting that the quantities are not directly comparable because the reported values are typically inferred from mass-transfer models and should be regarded as effective transport parameters. As such, they can embed assumptions about boundary-layer thickness and may implicitly include convection-enhanced mass transfer rather than representing purely diffusive transport. In contrast, the diffusivities reported in this work are profile-based effective chemical inter-diffusivities obtained from B-M analysis. They quantify the rate at which the concentration field evolves within the near-interface boundary layer along the experimental composition path under diffusion-dominated conditions. Despite these differences, the trends are qualitatively consistent with

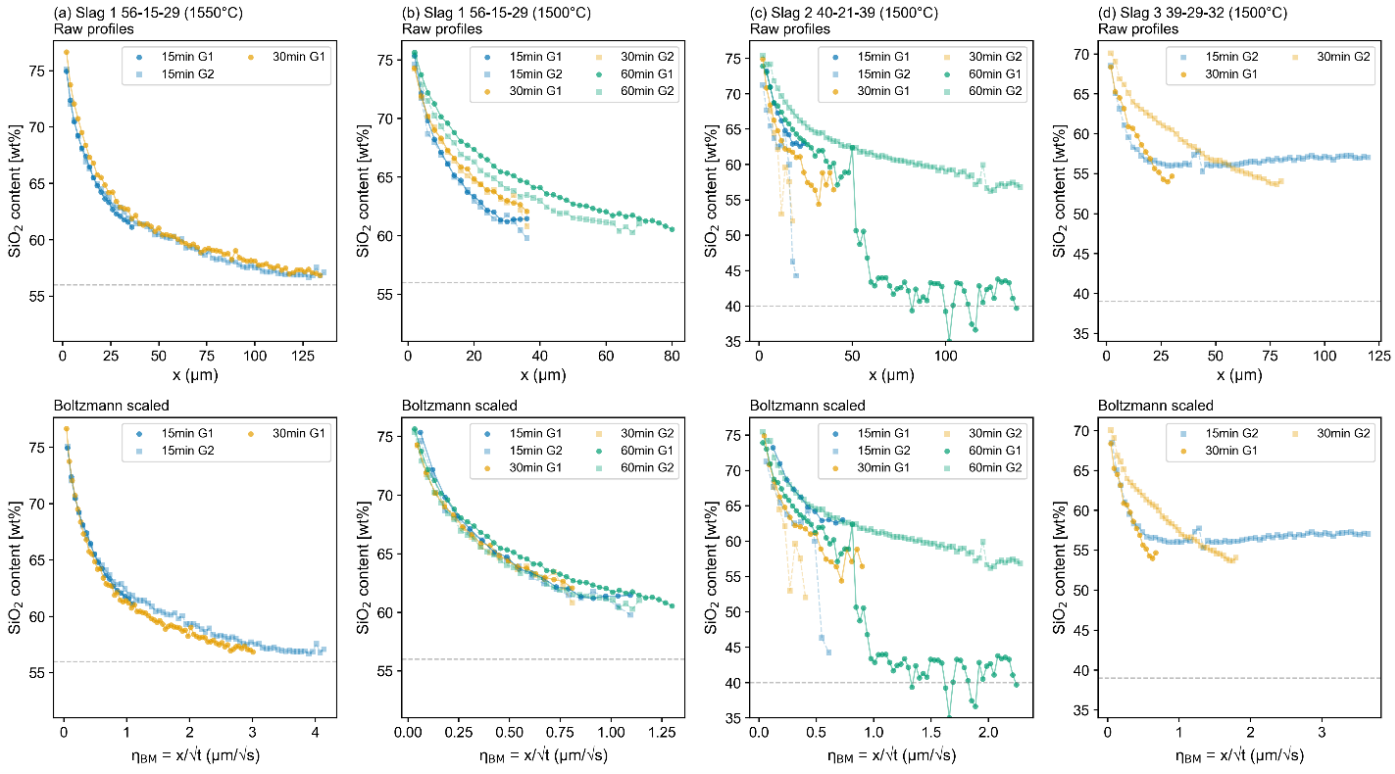

Figure 6— The Boltzmann–Matano screening summary for SiO2 dissolution profiles in studied slag

viscosity-controlled dissolution kinetics, in which higher-viscosity melts exhibit reduced mobility and lower effective transport coefficients.

Figure 8 shows the obtained apparent activation energy variation for Slag 1, where the viscous flow activation energy was obtained using the Zhang–Chou viscosity model (Zhang et al., 2014). It can be seen that both the apparent activation energy of the profile-based chemical inter-diffusivity and the activation energy of viscous flow decrease as SiO_2 content decreases. In addition, inter-diffusion values appear to drop more rapidly, suggesting that the two trends may converge and potentially cross in the low-SiO_2 region. It is also seen that the inter-diffusion activation energies remain systematically higher than those associated with viscous flow over the calculated composition range. Although experimental uncertainty cannot be excluded given the two-temperature estimate and the sensitivity of B–M inversion, the overall trend is still physically plausible. The reason is that the extracted effective chemical inter-diffusivity can reflect both kinetic mobility, which is strongly controlled by melt structure and viscosity, and thermodynamic driving-force contributions. As a result, its temperature dependence can be stronger than that of viscous flow alone, because changes in temperature affect not only the mobility of species in the melt but also the chemical-potential gradients that drive the re-establishment of chemical equilibrium along the composition path.

The temporal evolution of the SiO_2 concentration field was modelled for Slag 1. Figure 9 shows the predicted SiO_2 concentration profiles as a function of distance from the SiO_2/slag interface at increasing times. The results indicate that SiO_2 dissolution into the SiO_2-CaO-Al_2O_3 slag system is a relatively slow process. When considering the industrial silicon production process, the residence time of raw materials within the furnace must be considered. Given the low diffusion coefficients obtained in this study, in the order of 10^{-12} m^2/s – 10^{-13} m^2/s, diffusion-controlled equilibration is inherently slow. While industrial convection and mixing can accelerate mass transfer, day-scale contact times are still likely required to approach full equilibrium with quartz at 1500 °C, particularly in weakly mixed or stagnant regions.

Considering these slow rates, it is unlikely that descending slags have sufficient time to reach SiO_2 concentration of 70% – 80% purely through dissolution in the furnace. However, accumulated slag is likely to remain for a significantly longer duration. As quartz is continuously fed from the top of the furnace, the accumulated slags will have prolonged access to SiO_2. Under the assumption that the slag remains in inactive zones, it will gradually dissolve more SiO_2 until it reaches higher concentrations. Furthermore, as viscosity increases with both decreasing temperature and increasing SiO_2 content, the slag becomes more resistant to flow and is then more likely to accumulate.

Varying amounts of SiO_2 in the slag affects its physical properties and, hence, also its behaviour within the furnace. Viscosity is one of the most critical factors influencing the slag flow through the furnace. It is preferable with sufficient low viscosity to ensure a good mass transport. It is found that the accumulated slag in the upper parts of the furnace generally has a higher SiO_2 content compared to the slag found further down, while the CaO/Al_2O_3 ratio is relatively constant within the same furnace (Folstad, 2023). Slag in the inactive zone typically contains > 50% SiO_2, whereas the SiO_2 content at the furnace bottom generally is generally < 50%. Figure 10 displays the slag viscosity on a logarithmic scale as a function of increasing SiO_2 content for a fixed CaO/Al_2O_3 ratio of 0.5. The corresponding compositions are indicated by the arrow in the SiO_2-CaO-Al_2O_3-phase diagram in the same figure. The viscosity curves from 1500 °C – 2000 °C show that the viscosity increases significantly with higher SiO_2 concentrations. This trend becomes even more pronounced with higher SiO_2 concentrations. Furthermore, because the liquidus temperatures are often higher than the actual expected temperatures in that area, the slag system may be only partly liquid. This partial solidification further increases the effective viscosity.

These data also indicate that the impact of SiO_2 concentration on viscosity is in the same size range as a temperature change of 500 °C. Since the slag in inactive zone of the furnace typically ranges from 50 – 80 wt%, the viscosities at 1500 °C will vary from approximately 25 000 cP – 1 000 000 cP – ranging from the consistency of ketchup to the glass 'working point'. With both higher SiO_2 content and lower temperatures, compared to the furnace bottom, the slag in the inactive zone becomes more viscous. This higher viscosity makes the slag more resistant to flow and more likely to accumulate, which is negative for the furnace operation.

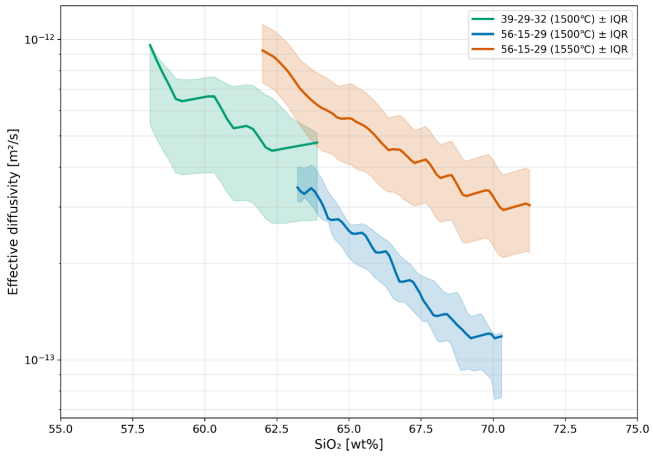

Figure 7—The concentration-dependent diffusivity for Slag 1 and 3 calculated using Boltzmann-Matano inversion of EPMA concentration profiles. Solid lines show the median concentration-dependent diffusivity D(C), and shaded bands indicate the interquartile range across profiles

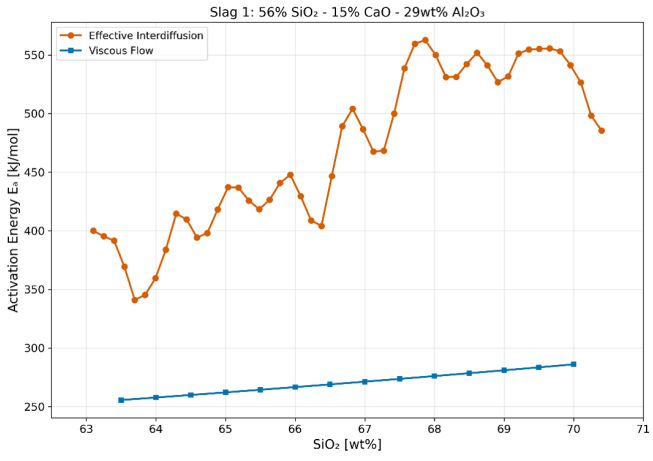

Figure 8—Apparent activation energy for the profile-based effective chemical inter-diffusion compared with the activation energy of viscous flow at the same SiO2 content

Dissolution of SiO_2 in SiO_2-CaO-Al_2O_3 slags

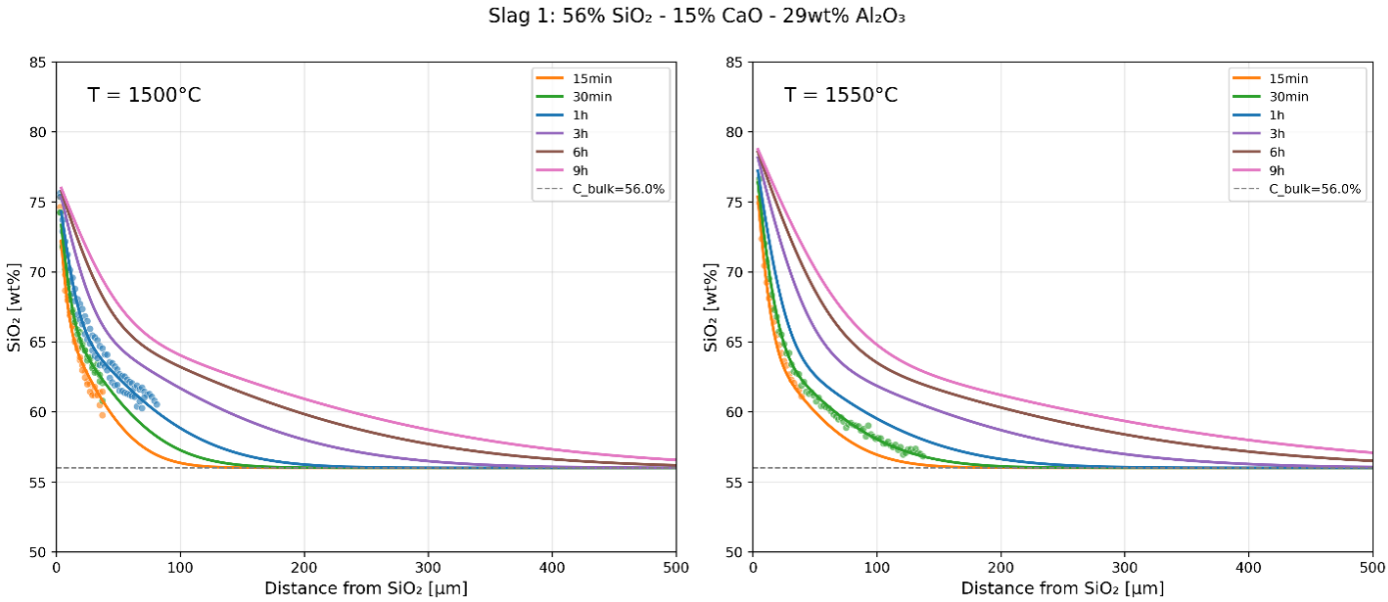

Figure 9—Estimated temporal evolution of SiO2 dissolution into Slag 1

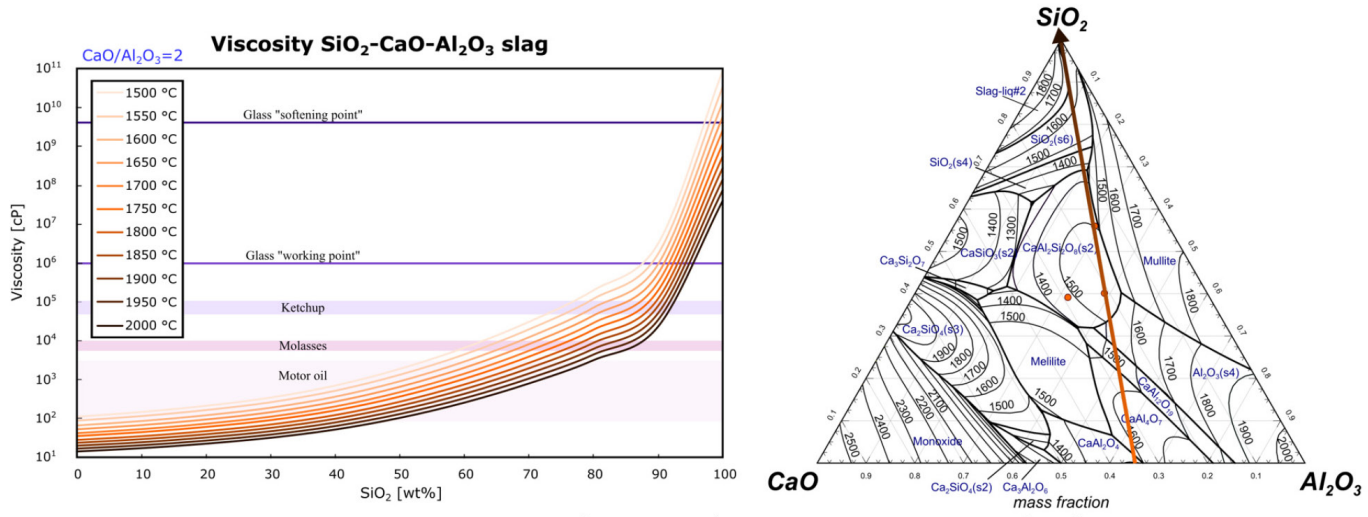

Figure 10—Viscosity as a function of SiO2 concentration in the slag

Conclusions

This study investigated the SiO_2 dissolution into different three SiO_2-CaO-Al_2O_3 slag compositions relevant for Si production. The measured profiles exhibit a growing near-interface SiO_2-enriched boundary layer and a stable far-field plateau, consistent with diffusion-dominated concentration-field evolution over the investigated length scale. Boltzmann self-similarity screening supports the use of B–M inversion to extract a profile-based effective chemical inter-diffusivity, which decreases systematically with increasing SiO_2 content and falls on the order of ~10^{-12} m^2/s – 10^{-13} m^2/s over the resolved composition range, with higher values at higher temperature. The interdiffusion activation-energy trends suggest that, in the SiO_2-rich region, thermodynamic driving-force contributions may play an important role. The low diffusivities imply intrinsically slow diffusion-controlled enrichment, making it unlikely that descending slags reach equilibrium within typical furnace residence times.

Acknowledgements

The authors would like to thank The Norwegian Ferroalloy Research Association (FFF) and the Norwegian Research Council (NRC) for their financial support through the KBN project Recursive, project no 326581.

References

Crank, J. 1979. The Mathematics of Diffusion, 2nd edn. Oxford University Press, Oxford.

Feichtinger, S., Michelic, S.K., Kang, Y.–B., Bernhard, C. 2014. In Situ Observation of the Dissolution of SiO_2 Particles in CaO-Al_2O_3-SiO_2 Slags and Mathematical Analysis of its Dissolution Pattern. *Journal of the American Ceramic Society*, vol. 97, no.1, pp.316–325.

Folstad, M.B. 2023. Slag and its effect on Si and FeSi production. PhD Thesis, Norwegian University of Science and Technology, Trondheim.

Folstad, M.B., Tangstad, M. 2021. SiO_2-CaO-Al_2O_3 slags in the Si/FeSi furnaces. Proceedings of INFACON XVI. *The Southern African Institute of Mining and Metallurgy*. Trondheim.

Franzefoss Minerals AS. 2024. https://kalk.no/en/ (accessed on 8.1.24).

Gou, L., Liu, H., Ren, Y., Zhang, L. 2023. Concept of Inclusion Capacity of Slag and Its Application on the Dissolution of Al_2O_3, ZrO_2 and SiO_2 Inclusions in CaO–Al_2O_3–SiO_2 Slag. *Metallurgical and Materials Transactions B*, vol. 54B, no.3, pp.1314–1325.

Heo, J., Park, J.H. 2022. Effect of temperature on the slag/refractory interfacial reaction with directed reduced iron (DRI) addition in an electric arc furnace (EAF) process: Diffusional growth of magnesiowüstite layer by Boltzmann-Matano analysis. *Ceramics International*, vol. 48, no. 12, pp. 17217-17224.

Johansen, S.T., Tveit, H., Grådahl, S., Valderhaug, A., Byberg, J.Å. 1998. Environmental aspects of Ferro-Silicon furnace operations - an investigation of waste gas dynamics. *Proceedings of INFACON VIII. Beijing, China*.

Jusnes, K.F. 2020. Phase transformations and thermal degradation in industrial quartz. *PhD Thesis*, *Norwegian University of Science and Technology*, Trondheim.

Jusnes, K.F., Hjelmseth, R., Folstad, M.B., Ditlefsen, N.S., Tangstad, M. 2021. Investigation of slag compositions and possible relation to furnace operation of a FeSi75 furnace. Proceedings of INFACON XVI. *The Southern African Institute of Mining and Metallurgy*. Trondheim.

Kadkhodabeigi, M. 2011. Modeling of Tapping Processes in Submerged Arc Furnaces. *PhD Thesis*, Norwegian *University of Science and Technology*, Trondheim.

Kristiansen, S. 2022. Dissolution rate and wettability of SiO_2–CaO–Al_2O_3 slag on quartz. *Project work*, *Norwegian University of Science and Technology*, Trondheim.

Kristiansen, S. 2023. Dissolution Rate and Wettability of SiO_2-CaO-Al_2O_3 Slags on Quartz. *Master Thesis*, *Norwegian University of Science and Technology*, Trondheim.

Ksiazek, M. 2018. Report: Excavation of Si furnace at Elkem Salten. Report No. 2018:00692. SINTEF, Trondheim.

Ksiazek, M., Saadieh, R., Gaertner, H., Grådahl, S., Sægrov, B., Tangstad, M., Valderhaug, A., Ringdalen, E. 2021. Industrial measurements of the gas and temperature in Si and FeSi production process. Proceedings of INFACON XVI. *The Southern African Institute of Mining and Metallurgy*. Trondheim.

Ksiazek, M., Tangstad, M., Ringdalen, E. 2013. Five furnaces five different stories. *Silicon for the Chemical and Solar Industry XIII*. pp. 33–42.

Ksiazek, M., Tangstad, M., Ringdalen, E. 2018. The rapid Si-furnace excavation - an unique chance to investigate the interior of the furnace. Proceedings of INFACON XV. Cape Town.

Majdič, A. and Wagner, H. 1970. Diffusion of Silicon in Molten Lime-Silica-Alumina Slags. Archiv für das Eisenhüttenwesen, vol. 41 no. 6, pp. 529–532.

Myrhaug, E. 2020. KPN CONTROLLED TAPPING, Examples of conceptual models based on simplified COMSOL simulations. Industrial presentation from Elkem ASA, KPN Controlled Tapping Meeting 2020.03.05.

Oishi, Y., Cooper Jr., A.R., Kingery, W.D. 1965. Dissolution in Ceramic Systems: III, Boundary Layer Concentration Gradients. *Journal of the American Ceramic Society*, vol. 48, no.2, pp 88–95.

Ren, Y., Zhu, P., Ren, C., Liu, N. and Zhang, L. 2023. Dissolution of SiO2 Inclusions in CaO-SiO2-Based Slags In Situ Observed Using High-Temperature Confocal Scanning Laser Microscopy. *Metallurgical and Materials Transactions* B, vol. 53 no. 2, pp. 682–692.

Samaddar, B.N., Kingery, W.D., Cooper Jr., A.R. 1964. Dissolution in Ceramic Systems: II, Dissolution of Aluminu, Mullite, Anorthite, and Silica in a Calcium-Aluminum-Silicate Slag. *Journal of the American Ceramic Society*, vol. 47 no. 5, pp. 249–254.

Schei, A., Tuset, J.Kr., Tveit, H. 1998. Production of High Silicon Alloy. Tapir, Trondheim.Tangstad, M., Ksiazek, M., Andersen, J.E. 2014. Zones and Materials in the Si Furnace. Silicon for the Chemical and Solar Industry XII. Trondheim, Norway.

ThermoFisher Scientific. 2024. https://www.thermofisher.com/no/en/home.html (accessed on 8.1.24.

Tranell, G., Andersson, M., Ringdalen, E., Ostrovski, O., Steinmo, J.J. 2010. Reaction zones in a FeSi75 furnace – results from an industrial excavation. *Proceedings of INFACON XI*I. Helsinki. pp. 709–715.

Zhang, Guo-Hua, Kuo-Chih Chou, and Ken Mills. "A structurally based viscosity model for oxide melts." *Metallurgical and Materials Transactions B* 45.2 (2014): pp. 698-706. ◆